Please cite this article in press as: Svirinovsky-Arbeli et al., Using NMR spectroscopy to link structure to function at the Li solid electrolyte interphase, Joule (2024), https://doi.org/10.1016/j.joule.2024.04.016

Joule

CellPress

Perspective

Using NMR spectroscopy to link structure to function at the Li solid electrolyte interphase

Asya Svirinovsky-Arbeli,[1] Mikkel Juelsholt,[1] Richard May,[2] Yongbeom Kwon,[1] and Lauren E. Marbella[1,*]

SUMMARY

The performance of Li metal batteries is tightly coupled to the composition and properties of the solid electrolyte interphase (SEI). Even though the role of the SEI in battery function is well understood (e.g., it must be electronically insulating and ionically conductive, it must enable uniform Li^+ flux to the electrode to prevent filament growth, it must accommodate the large volume changes of Li electrodeposition), the challenges associated with probing this delicate composite layer have hindered the development of Li metal batteries for practical applications. In this review, we detail how nuclear magnetic resonance (NMR) spectroscopy can help bridge this gap in characterization due to its unique ability to describe local structure (e.g., changes in crystallite size and amorphous species in the SEI) in conjunction with ion dynamics while connecting these properties to electrochemical behavior. By leveraging NMR, we can gain molecular-level insight to aid in the design of Li surfaces and enable reactive anodes for next-generation, high-energy-density batteries.

INTRODUCTION

Li metal batteries (LMBs) promise to enable long-range electric vehicles and offer the potential to electrify heavy-duty trucks and small aircraft.[1–3] However, to utilize high-energy-density LMBs, we must minimize Li inventory through the use of thin Li metal anodes and small electrolyte volumes.[4] These requirements present a problem in liquid electrolytes because the low potential of Li metal (−3.04 V vs. standard hydrogen electrode [SHE]) leads to the consumption of that Li inventory to form the solid electrolyte interphase (SEI).[5,6] To minimize Li losses, the SEI that passivates the Li surface should be thin while still allowing reversible ion transport and electrodeposition and remaining impermeable to electrons. Any lateral heterogeneity across the electrode surface, either from the SEI or the metal itself, may create uneven Li^+ distribution and localized areas of increased current density. High-surface-area Li filaments can grow at these "hot spots" and, upon stripping, create electrochemically inactive Li^0, leading to additional Li losses and low Coulombic efficiency (CE).

The stringent demands on Li metal surface chemistry call for electrolyte formulations that can achieve >99.99% CE. Improvements in Li CE are linked to specific changes in SEI chemistry that may be characterized via advanced surface analytical tools such as X-ray photoelectron spectroscopy (XPS), Fourier transform infrared spectroscopy (FTIR), nuclear magnetic resonance (NMR) spectroscopy, and mass spectrometry (MS).[7–9] For example, the boost in CE observed when using fluorinated derivatives

CONTEXT & SCALE

Li metal batteries (LMBs) offer higher energy density than conventional Li^+ batteries, making them suitable for game-changing applications like aviation. However, LMBs are plagued by interfacial interactions that lead to irregular Li deposits and low Coulombic efficiency (CE). Advancing LMBs involves enhancing CE through electrolyte engineering to alter the structure and properties of the solid electrolyte interphase (SEI). A robust SEI layer prevents further decomposition of the electrolyte, promotes Li^+ diffusion, and enables reversible Li cycling. However, a thorough correlation between SEI properties and cell function has yet to be established. Nuclear magnetic resonance (NMR) spectroscopy is a powerful tool to establish this link because it can simultaneously characterize ion dynamics (e.g., ion hopping in a single phase or movement across interfaces) and local ion coordination environment at the atomic scale.

Here, we highlight work where NMR is used to measure SEI properties, including Li^+ exchange, passivation stability, and energy barriers to Li^+ diffusion, while also providing detailed information on the composition and structure of SEI phases. We discuss how NMR

Please cite this article in press as: Svirinovsky-Arbeli et al., Using NMR spectroscopy to link structure to function at the Li solid electrolyte interphase, Joule (2024), https://doi.org/10.1016/j.joule.2024.04.016

of battery solvents, like fluoroethylene carbonate (FEC), is correlated with the presence of LiF and polymerized vinylene carbonate (poly(VC)) molecules in the SEI.[10–12] These components offer better stability over conventional cyclic and linear carbonate solvents that predominantly decompose to form a mixture of organic small molecules (e.g., lithium ethylene dicarbonate [LEDC]) and in some electrolyte formulations deleterious salt decomposition products (e.g., HF and PF_5).[13,14] Further gains in CE can be attained by moving to ether-based solvents, especially when used in combination with electrolyte salt mixtures containing lithium bis(trifluoromethanesulfonyl)imide (LiTFSI), lithium bis(fluorosulfonyl)imide (LiFSI), and $LiNO_3$.[15–21] Analysis of the SEIs produced in these electrolytes indicates that these layers decrease in thickness and contain high quantities of inorganic compounds (e.g., LiF, Li_2O, and $Li_xN_yO_z$) and very little organics.[15,16,19,21,22]

Although the development of cutting-edge characterization methods has considerably improved our understanding of the composition and arrangement of the SEI, building structure-property-performance relationships has been much more challenging. First, the structural and mechanical properties of the nanoscale compounds in the SEI may not correspond to the bulk form of their compounds, making it difficult to link composition with physical properties. Second, many of the spectroscopic methods that report on SEI composition and structure do not provide information on interfacial properties, like electrochemical kinetics or interfacial resistance (e.g., action of ions associated with an electrochemical reaction or mass transfer through an interphase), requiring distinct chemical and electrochemical measurements and models to correlate the separate datasets. Third, discrete phases embedded in the SEI are often intermixed and disordered, which presents issues with parsing individual and synergistic contributions to function even if they can be characterized. Ideally, we want to perform compositional, structural, and property analysis of the SEI using a single approach so that we can perform these measurements on the same sample and directly relate these features to Li CE and deposition morphology.

NMR spectroscopy is a powerful tool to connect SEI structure with interfacial phenomena in LMBs because it is one of the only techniques that can simultaneously characterize ion dynamics and local ion environment. The battery literature is rapidly growing with examples where NMR is used to quantitatively measure dynamic processes at interfaces *in situ*, such as Li exchange and corrosion local to electrode surfaces, in conjunction with traditional electrochemical techniques.[22–34] In the NMR experiment, we can gather information on the composition and structure of the electrolyte, SEI, and electrode with high chemical and, in certain scenarios, spatial resolution.[10,22,35–42] These compositional diagnostics are particularly sensitive to light elements and can detect both amorphous and crystalline regions of the sample. When NMR is used in conjunction with electrochemical methods, XPS, MS, FTIR, electron microscopy (EM), and computer simulations, we can provide a compelling visualization of interfaces in batteries and how certain structures impact Li^+ transport.

In this review, we demonstrate how NMR is used to measure SEI properties, including Li-ion exchange, passivation stability, and barriers to Li^+ diffusion, while also providing detailed information on the composition and structure of SEI phases. We start by orienting the reader to traditional electrochemical methods, like voltammetry and electrochemical impedance spectroscopy (EIS), that have been used to correlate the electrochemical behavior of Li electrodes (such as Li exchange current and electrode potential) with CE and its relationship to the SEI.[43–47] Next, we discuss NMR methods that can also measure Li exchange across interfaces and the

complements electrochemical approaches to reveal the molecular-level origin for this dynamic behavior. By coupling NMR with other analytical and electrochemical tools, we may improve our understanding of specific SEI compounds and their properties (e.g., how ionically insulating compounds like LiF allow Li ions to transverse the SEI) that enhance cell performance and expand this knowledge to the rational design of LMBs.

[1]Department of Chemical Engineering, Columbia University, New York, NY 10027, USA

[2]Department of Earth & Environmental Engineering, Columbia University, New York, NY 10027, USA

*Correspondence: lem2221@columbia.edu

https://doi.org/10.1016/j.joule.2024.04.016

Please cite this article in press as: Svirinovsky-Arbeli et al., Using NMR spectroscopy to link structure to function at the Li solid electrolyte interphase, Joule (2024), https://doi.org/10.1016/j.joule.2024.04.016

associated energy barriers to provide analogous data along with insight into the relationship between electrochemically active Li^0 (or cyclable Li^0) and SEI composition, growth, and permeability.[22–24,27] With a better understanding of SEI dynamics, we then examine how NMR can be used in combination with other approaches (e.g., cryoEM, computational modeling, and time-of-flight secondary ion mass spectroscopy [TOF-SIMS]) to provide deeper insight into the structures that dictate Li diffusion as well as the precise mechanisms behind Li transport through the multicomponent SEI.[48–52] Overall, the ability to construct SEI structure-property-performance relationships will equip us to rationally design electrolytes that not only enable rechargeable LMBs but also allow us to build on that knowledge to create entirely new, highly tailorable systems.

CONNECTING ELECTROCHEMICAL DESCRIPTORS FOR HIGH-CE LI METAL ANODE ELECTROLYTES TO LI SEI

Some of the most intense research efforts over the past several decades have been dedicated to improving the CE of Li metal anodes through electrolyte engineering, which inherently impacts the SEI.[53,54] Due to the highly reactive nature of Li metal, Li inventory is lost to the SEI or electrochemically inactive Li^0 during cycling, and CE in these systems has never reached the 99.99% target required for practical lifetimes.[55,56] To achieve this goal, Li losses will likely have to be primarily SEI-based, highlighting the importance of this layer in designing Li metal anodes. At present, electrolyte engineering in the form of increased salt concentration,[15,18,57–59] localized high-concentration electrolytes (LHCEs),[60–62] $LiNO_3$ or LiFSI addition,[16,17] and liquefied gas electrolytes[63] often results in Li CEs > 98% as summarized in Figure 1A. However, the commonalities between these vastly different electrolyte formulations that enable reversible Li deposition are not entirely clear. As a result, researchers have been searching for a way to link Li metal CE with electrolyte-dependent properties such as charge-transfer kinetics,[43,44,64–67] SEI resistance and composition,[43,68,69] Li exchange,[22–24,46] and Li electrode potential (E_{Li})[43,47] that would allow rapid screening of new electrolyte formulations. Unfortunately, there is still a great deal of debate about how these features correlate with the reversibility and preservation of electrochemically active Li^0 (e.g., both high and low exchange current density are linked to high CE; thick and thin SEI are both tied to high-performing anodes). These discrepancies may be due to the reactivity of Li metal, different experimental protocols, different cell pressures and glovebox conditions, and other lab-to-lab variabilities.

Given the sensitivity of Li metal to analysis conditions, it is critical that different electrolytes be compared within the same laboratory, using the same test conditions. To this end, Cui and coworkers have examined 17 different electrolyte formulations using transient cyclic voltammetry (CV) with ultramicroelectrodes (dimensions <20 μm) and found that exchange current density (j_0 ranging from 2.4–66 mA/cm^2) exhibits a positive correlation with CE between 79.6%–98.3% as shown in Figure 1C.[43] In this case, the use of ultramicroelectrodes allows the user to measure the exchange current density at fresh Li/electrolyte interfaces in the absence of SEI. When analyzing the properties of the native SEI with EIS, the authors found that the SEI resistance of pre-cycled Li/Li symmetric cells was not related to cyclable Li^0. They argue that Li^+ solvation structure and E_{Li} ultimately control the relationship between electron transfer and Li deposition morphology, where weakly coordinating solvents facilitate smooth plating. Here, altering the solvation structure changes the chemical potential of Li^+ in the electrolyte, which leads to well-documented variations in E_{Li} as a function of solvent.[70,71] These findings are consistent with a comprehensive study

Please cite this article in press as: Svirinovsky-Arbeli et al., Using NMR spectroscopy to link structure to function at the Li solid electrolyte interphase, Joule (2024), https://doi.org/10.1016/j.joule.2024.04.016

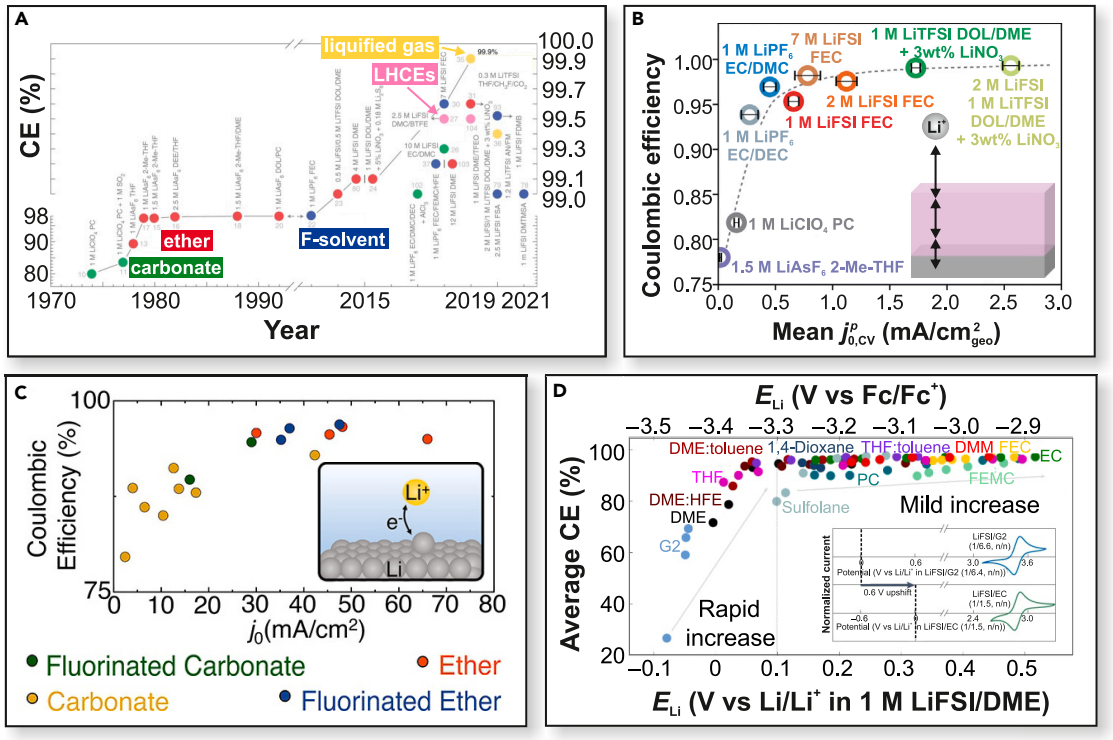

Figure 1. Correlation between electrolyte formulation, Li metal CE, and electrochemical properties

(A) For over 5 decades, the development of ether solvents, fluorinated solvents, high-concentration Li salts, localized high-concentration electrolytes, and liquified gas electrolytes to replace conventional carbonate electrolytes with low-concentration (1 M) Li salts has enabled Li metal CE to improve from ~80% to >99%. Adapted with permission from Hobold et al.,[55] Copyright 2021 Springer Nature Limited.

(B) Positive correlation between $j^{p}_{0,CV}$ and CE for 9 different electrolytes, including low-concentration carbonates, ethers, fluorinated carbonates, high-concentration electrolytes, and $LiNO_3$-containing systems. Error bars in the figure denote the standard deviation over 11 cycles. Adapted with permission from Hobold et al.,[46] Copyright 2023 Royal Society of Chemistry.

(C) Positive correlation between $j_{0,CT}$ and CE for 17 different electrolytes, including fluorinated carbonates, ethers, carbonates, and fluorinated ethers. Adapted with permission from Boyle et al.,[43] Copyright 2022 American Chemical Society.

(D) Positive correlation between E_{Li} and average CE for 74 different electrolytes spanning carbonates, ethers, fluorinated solvents, and sulfolanes. Adapted with permission from Ko et al.,[47] Copyright 2022 Springer Nature.

by Yamada and coworkers who investigated the relationship between E_{Li} and CE in 74 different electrolytes (Figure 1D).[47] In this work, the authors use machine learning, vibrational spectroscopy, and electrochemical measurements to support the idea that Li^+-anion pairs in the electrolyte are associated with large shifts (>0.6 V) in E_{Li} that improve interfacial instability and increase CE. Taken together, both of these studies indicate that screening electrolytes for high E_{Li} can be used to predict Li^0 cyclability. By contrast, the native SEI on Li metal chips is likely subject to too many variables (e.g., user handling, daily glovebox conditions) to be a good indicator of CE in a given electrolyte. However, we know that normal battery operation will cause this native layer to change and form a new SEI that modulates Li^+ transport between the electrolyte and the underlying electrode that will impact performance. The value of E_{Li} is linked to the SEI formed upon cycling because it is a direct indicator of the reducing ability of Li metal. High-CE electrolyte formulations that exhibit increased values of E_{Li} are expected to exhibit low amounts of reductive decomposition, but a Li SEI layer will always be present, and the compounds in the SEI will also shift as one changes electrolyte, which can impact Li deposition behavior. For example, many of the electrolytes that show large increases in E_{Li} often form contact-ion pairs that are correlated with anionic-based decomposition products (e.g., LiF) in the SEI, and the

role of these products is not well known. Understanding how the SEI impacts electrochemical kinetics, Li^+ transport, Li^+ (de)solvation, and the interplay between these variables is critical to controlling Li metal battery performance.

Gallant and coworkers proposed that Li exchange in the presence of the SEI is more aptly described by a pseudo-exchange current density (j_0^P) that is probed with slow voltammetry (1 mV/s) and EIS measurements that capture the total rate of Li^+ exchange, including both mass transport and charge-transfer kinetics.[46] In this case, Li exchange refers to the exchange of Li between the electrode and the SEI as well as Li movement through the SEI and exchange with the electrolyte (Figure 1B). Results from CV and EIS show a positive correlation between Li exchange and CE for both low CE and high-CE electrolytes (for 9 different systems ranging from 78.0%–99.0%, Figure 1B). The precise j_0^P values measured in these systems have important implications for the rate capabilities of LMBs. Low CE electrolytes (<97%, mostly carbonate solvents, e.g., propylene carbonate [PC], ethylene carbonate/diethyl carbonate [EC/DEC], and ethylene carbonate/dimethyl carbonate [EC/DMC]) showed moderate, constant Li j_0^P values (< 1 mA/cm^2) during cycling, indicating that they must be operated at low current densities to avoid excessive filament growth during Li metal stripping/plating. By contrast, high-CE electrolytes (>97%, generally concentrated solutions, and ethers containing $LiNO_3$) exhibited j_0^P values that increase as a function of cycle number (>5 mA/cm^2), suggesting that Li exchange is not the rate-limiting step to fast cycling. Insight into how the SEI chemistry changes as a function of electrochemical cycling to increase Li exchange may help construct high-performance LMBs.

CONNECTING LI EXCHANGE TO SEI STRUCTURE AND SEI PROPERTIES WITH NMR

Here, NMR spectroscopy is particularly helpful because it provides information on Li exchange behavior in parallel with (1) microscopic SEI properties and (2) the arrangement of chemical compounds on the Li surface. In 2018, Jerschow and coworkers showed that isotopically enriched ^{6}Li metal electrodes simply placed in natural abundance ^{7}Li electrolyte in a solution NMR tube could be used to monitor SEI growth and the exchange of Li^+ between the metal surface and the electrolyte at open circuit voltage (OCV) with ^{7}Li NMR.[28] This experiment is elegant in the sense that it is relatively straightforward; by monitoring the change in NMR signal intensity for a given isotope in one of the two phases (i.e., solid metal electrode and liquid electrolyte), one can quantify Li^+ exchange rate and SEI growth rate simultaneously. Leveraging this approach, Grey and coworkers identified how Li exchange is related to improved performance upon addition of 10% FEC to 1 M $LiPF_6$ in EC/DMC (LP30).[23] In this work, the authors followed the exchange rate of Li ions between ^{6}Li metal and natural abundance Li electrolyte (92% ^{7}Li) at OCV and developed a model to compare the rate of SEI growth, SEI permeability, and exchange current density between LP30 both with and without FEC. Figure 2A shows how the ^{7}Li NMR signal intensity of the metal increases as ^{7}Li from the electrolyte exchanges with the ^{6}Li-rich metal surface over time. Correspondingly, the ^{7}Li NMR signal from the electrolyte decreases. This exchange process between the electrode/electrolyte interface is fit to a four-parameter model that describes the initial isotope exchange flux of the first NMR measurement ($J_{ex,0}$), the SEI permeability constant, the SEI growth constant, and the SEI formation proportionality constant that captures SEI formation rate. The parameters associated with SEI formation indicate that interphase growth on Li metal is faster in the presence of FEC compared with LP30 alone. More rapid SEI growth implies that FEC-containing electrolytes immediately

Please cite this article in press as: Svirinovsky-Arbeli et al., Using NMR spectroscopy to link structure to function at the Li solid electrolyte interphase, Joule (2024), https://doi.org/10.1016/j.joule.2024.04.016

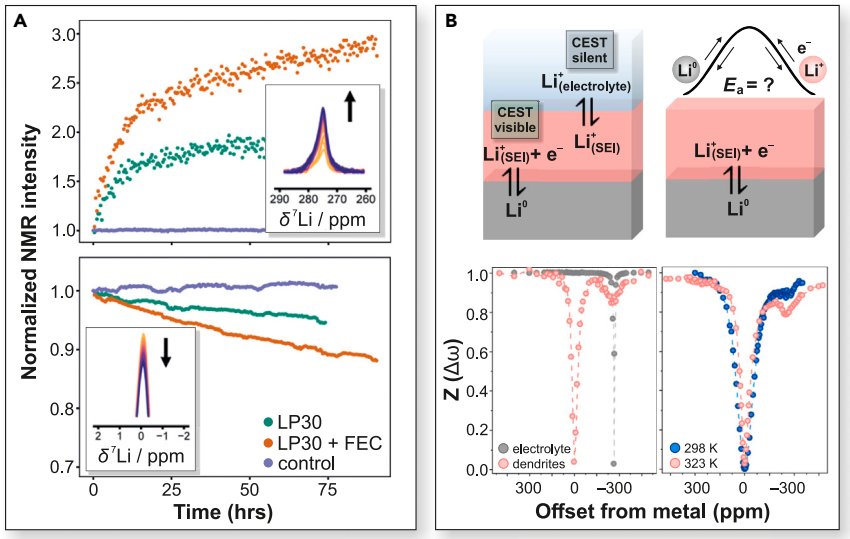

Figure 2. Suite of NMR techniques to simultaneously evaluate Li exchange and SEI properties for comparison with Li metal battery performance

(A) Normalized NMR signal intensities as a function of time measured during $^{6/7}$Li isotope exchange measurements for ^{6}Li metal (top) in natural abundance electrolyte (bottom, LP30 = green, LP30 + FEC = orange, control = purple with no isotopic enrichment) (adapted with permission from Gunnarsdóttir et al.,[23] Copyright 2020 Royal Society of Chemistry).

(B) Schematic of the physical processes probed with different ^{7}Li CEST experiments (top) and the corresponding Z-spectra in LP30 (bottom). The spectrum on the left shows a comparison of the Z-spectrum for the Li dendrites (pink) with that of the electrolyte (gray). The pink Z-plot shows the spectrum obtained after collecting the signal intensity of the Li dendrites (frequency offset of 0 ppm) as a function of saturation pulse irradiation at variable offsets. After irradiating the Li dendrites, there is a decrease in the broad signal that corresponds to the SEI (frequency offset −300 ppm). The Z-spectra on the right were acquired from the dendrite signal at T = 293 K (blue) and T = 323 K (pink) to calculate the activation energy for Li exchange. Adapted with permission from Columbus et al.,[24] Copyright 2022 American Chemical Society.

passivate the Li metal surface. Electrolyte formulations that exhibit fast growth rates with structurally and chemically stable SEI species (e.g., LiF and cross-linked poly [VC]) may also quickly repair the surface if the SEI is damaged during the large volume changes that occur during stripping/plating, minimizing electrolyte consumption during cycling. In addition, the isotope exchange experiment reveals that the SEI formed with FEC is less permeable to Li^+, suggesting that the reduction products also help protect the Li surface compared with the control electrolyte. By taking the product of $J_{ex,0}$ and Faraday's constant, the authors calculate an exchange current density from the $^{6/7}$Li isotope exchange measurements (j_0^{NMR}). From this calculation, they find that the exchange current with FEC (j_0^{NMR} = 0.030 mA/cm^2) is approximately twice that without FEC (j_0^{NMR} = 0.015 mA/cm^2), giving values that are consistent with results from EIS at OCV and ultimately showing that high-performance electrolytes are correlated with increased exchange current.

Similar to what was noted in the electrochemical studies discussed above, breakdown and reformation of the native SEI on Li metal likely impact the trajectory of Li metal CE over extended cycling. In some electrolytes, this process will eventually stabilize the Li surface, and in others, continuously poor passivation will lead to low CE. NMR techniques that can monitor Li^+ exchange during cycling allow us to understand how interfacial processes are coupled to (electro)chemical reactivity at the electrode surface. In 2022, Leskes and coworkers used ^{7}Li chemical exchange

saturation transfer (CEST) NMR experiments to detect and quantify the rate and energy barrier to Li^+ exchange between Li metal and the SEI *in situ*.[24] In this work, a Li/Li symmetric cell containing liquid electrolyte was placed inside of a 5 mm solution NMR tube. The sample was then polarized at ~3 mA/cm^2 for 4 h to grow Li filaments for ^{7}Li CEST NMR. In order to determine the environment of interfacial Li exchange probed with CEST, the authors varied the saturation frequency for the ^{7}Li resonance corresponding to Li dendrites (~270 ppm) vs. the liquid electrolyte (~0 ppm) and monitored the NMR signal intensity. The CEST NMR experiment is more complex, but in brief, it involves two exchangeable chemical environments (individual pools) that are spectrally resolved and plotted in a Z-spectrum. The CEST effect occurs when applying a saturation pulse to one pool, resulting in the disappearance of its signal. This, in turn, causes a decrease in signal intensity in the other pool if the two environments are undergoing exchange. Figure 2B shows the Z-spectra obtained by plotting the normalized signal intensity from a Li/Li symmetric cell. In the left panel of Figure 2B, the pink Z-plot shows the spectrum collected by monitoring the signal intensity of the Li metal environment (frequency offset of 0 ppm) as a function of saturation pulse irradiation at variable offsets. When the Li metal environment is irradiated, the authors observed a decrease in the broad signal that corresponds to the SEI (frequency offset −300 ppm). By contrast, looking at the Li electrolyte, when the environment for the electrolyte is saturated (gray Z-plot), there is no change in any of the other pools (i.e., we see no change in Z for the offset frequencies that correspond to the environments for Li metal or the SEI). These observations indicate that the exchanging environments are exclusively Li metal and SEI, and not Li metal and the electrolyte. Conducting the experiment at variable temperatures and fitting to the Arrhenius equation allowed the authors to extract the exchange rate and associated energy barriers.

When the authors measured the activation energy for Li exchange across the Li/SEI interface after cycling in LP30 electrolyte they found that it was 47 $\pm$ 2 kJ/mol.[24] This energy barrier is in line with the upper bound of nudged elastic band calculations that show Li^+ diffusion through defects in Li_2CO_3 is between 22 and 47 kJ/mol,[52] which is a major component of the SEI expected from a carbonate-based electrolyte.[72] Upon adding FEC to LP30, they found that the total rate of Li exchange at the metal/SEI interface increased from 64 to 91 s^{-1}, which is consistent with improvements in Li metal CE. This increase in Li exchange is the same trend that was observed prior to cycling by both Gunnarsdóttir et al. with NMR and EIS,[23] and Boyle et al. with ultrafast voltammetry.[44] Although this approach has only recently been applied to Li metal systems, this setup also offers the opportunity to observe electrolyte salt and solvent decomposition products *in situ* to further understand the reduction reactions that occur during Li stripping/plating.

Arguably the greatest benefit of performing Li exchange measurements in NMR is the ability to simultaneously capture both ion dynamics and SEI composition for the same sample, under the same conditions. In 2021, we investigated interfacial Li exchange in Li/Li coin cells cycled in both 0.5 M LiTFSI + 0.5 M $LiNO_3$ and 1 M LiTFSI in 1,3-dioxolane:dimethoxyethane (DOL:DME) electrolyte.[22] In this work, we measured Li-ion exchange rates between the Li metal electrode and the SEI after electrochemical cycling by extracting the anodes from Li/Li coin cells, removing the liquid electrolyte, and leaving behind an intact Li/SEI sample. From here, we used one- and two-dimensional (1D and 2D) exchange spectroscopy (EXSY) solid-state NMR, relaxation measurements, and XPS to identify the spatial arrangement of individual compounds in the SEI on Li metal as well as Li transport at the Li/SEI interface. In the EXSY NMR experiment, exchange between magnetically inequivalent

Please cite this article in press as: Svirinovsky-Arbeli et al., Using NMR spectroscopy to link structure to function at the Li solid electrolyte interphase, Joule (2024), https://doi.org/10.1016/j.joule.2024.04.016

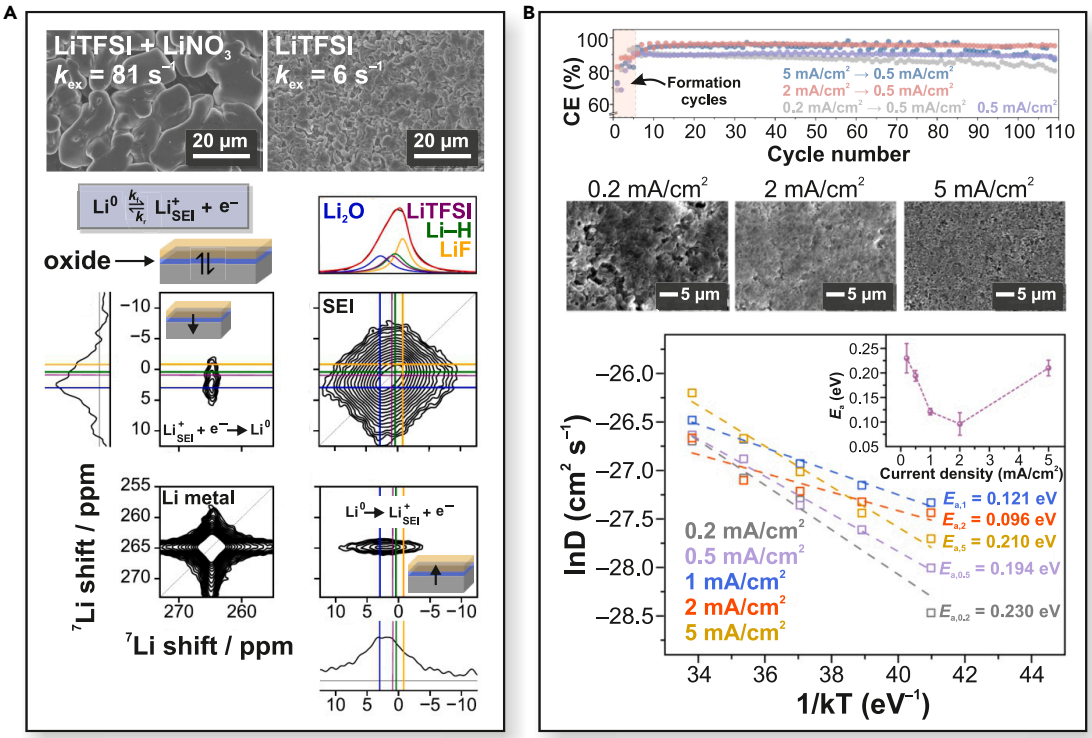

Figure 3. NMR exchange measurements correlate with exchange current density and obtain information on SEI composition and SEI properties

(A) SEM images of Li electrodeposits after galvanostatic polarization at 1 mA/cm^2 for 2 h in Li/Li cells in 0.5 M LiTFSI + 0.5 $LiNO_3$ (left, top) and 1 M LiTFSI (right, top) in DOL/DME electrolyte. The addition of $LiNO_3$ leads to lower surface area Li deposits and faster Li exchange rates, k_{ex}, as measured with 1D ^{7}Li EXSY NMR. The bottom spectrum corresponds to 2D ^{7}Li–^{7}Li EXSY NMR and individual 1D slices for the electrolyte decomposition products deposited on the surface of Li metal after cycling in 0.5 M LiTFSI + 0.5 M $LiNO_3$ in DOL/DME. The data indicate that Li_2O is located directly at the Li metal surface and thus participates in Li exchange between the SEI and the Li anode. Adapted with permission from May et al.,[22] Copyright 2021 American Chemical Society.

(B) Li CE as a function of cycle number (top) and Li deposition morphologies (middle) for different electrochemical formation protocols, where formation at 2 mA/cm^2 leads to the highest CE upon subsequent cycling at 0.5 mA/cm^2 at ~96% over the next ~100 cycles. 1D ^{7}Li EXSY NMR results (bottom) indicate that five formation cycles at 2 mA/cm^2 lead to the lowest activation energy for Li diffusion compared with higher (5 mA/cm^2) and lower current densities (1, 0.5, and 0.2 mA/cm^2). Error bars shown on the inset represent the standard error of the fitted data from the experiment. Adapted with permission from Zhang et al.,[27] Copyright 2024 American Association for Advancement of Science.

(i.e., spectrally resolved) environments is measured at different mixing times that represent the duration that the two sites undergo exchange. In a 2D EXSY NMR experiment, cross-diagonal peaks emerge when there is exchange between the two sites. In a 1D EXSY NMR experiment, the signal intensity of the sites may increase/decrease with mixing time.

Using this approach, we found that the addition of $LiNO_3$ to LiTFSI in DOL/DME was correlated with faster ion exchange (k_{ex} = 81 vs. 6 s^{-1}), higher CE (97% vs. 45% after 100 cycles), and smoother Li deposits compared with LiTFSI alone (Figure 3A), consistent with the aforementioned EIS and CV measurements. In all electrolytes, NMR indicated that the Li metal electrodes were covered in a layer of Li_2O (Figure 3A) that exhibited an activation energy of 15 $\pm$ 7 kJ/mol for interfacial Li exchange. Density functional theory (DFT) calculations predict that vacancy diffusion in Li_2O has an energy barrier of 15 kJ/mol,[52] which is less than half that of Li_2CO_3 or LiF. Yet, ionic transport in the SEI is only one aspect of functionality. *Ab initio* calculations also suggest that Li_2O at the Li surface is electronically insulating, especially compared with other reduction products that may be produced from separate

electrolyte components in our study, like Li_3N derived from $LiNO_3$.[73] With a mixture of species that exhibit different ionic and electronic conductivities, their relative location in the SEI can not only play an important role in battery performance to protect from continuous electrolyte reduction but also facilitate ion transport (note that ionic and electronic conductivity are often correlated). After cycling in the presence of $LiNO_3$, NMR and XPS show that the SEI on Li metal exhibits a multilayer architecture (as opposed to a mosaic structure) that contains more ionically conductive compounds on top of the initial Li_2O layer, e.g., $Li_xN_yO_z$, that is then coated with electronically insulating electrolyte reduction products (e.g., LiF). At present, one of the biggest open questions is the role that disorder and grain boundaries between these layers may play in altering the properties of the SEI and ultimately in Li electrodeposition (see the following section for a more in-depth discussion). Similar layered structures have been observed on the surface of Li metal with cryogenic transmission EM (cryo-TEM) after cycling in other high-performance electrolytes (e.g., LiPON, ethers, and FEC additives), whereas unfluorinated carbonates tend to form mosaic structures.[74–76] The combination of NMR and imaging data suggests that multilayer SEIs with higher quantities of conductive species enable smoother Li plating due to a more uniform flux to the Li metal surface at current densities commonly used in electrochemical testing (0.5–1 mA/cm^2).

Recently, Wagemaker and coworkers used ^{7}Li EXSY and solid-state NMR techniques to analyze how electrochemical formation protocols impact Li exchange, SEI composition, and Li metal cyclability.[27] In this work, the authors examined three different formation procedures where Li/Cu cells are cycled in LP30 at an initial current density (0.2, 2, or 5 mA/cm^2) for five cycles and then cycled at 0.5 mA/cm^2 for longer-term testing. All cells were compared with a control that was cycled at a constant current density of 0.5 mA/cm^2. Upon extended cycling at 0.5 mA/cm^2, the Li anode formed at 2 mA/cm^2 showed the lowest overpotential at ~40 mV during stripping/plating compared with those formed at 0.2 mA/cm^2 (~100 mV), 0.5 mA/cm^2 (~100 mV), or 5 mA/cm^2 (~70 mV). When the authors measured the CE of Li metal formed at 2 mA/cm^2 and cycled for 100 cycles at 0.5 mA/cm^2, they found that it reached an average of ~96% (Figure 3B), which is much higher than one might expect for LP30 (see Figure 1A). The other formation protocols produced CE values that were much more consistent with conventional carbonate electrolytes, where 0.2 and 0.5 mA/cm^2 formation steps resulted in a CE of ~80% and 88%, respectively, while 5 mA/cm^2 led to inconsistent values but was mostly around ~90% (Figure 3B).

To understand how electrochemical formation alters subsequent Li electrodeposition, the authors performed variable-temperature 1D ^{7}Li EXSY NMR to extract the activation energy of interfacial Li diffusion (Figure 3B). From this experiment, they found that the activation energy for Li diffusion at the SEI/metal interface when the anodes were formed at 2 mA/cm^2 of E_a = 9.3 kJ/mol. This energy barrier is significantly lower compared with electrodes that are formed at both lower (E_a [0.2 mA/cm^2] = 22 kJ/mol, E_a [0.5 mA/cm^2] = 19 kJ/mol) and higher (E_a [5 mA/cm^2] = 20 kJ/mol) current densities. These data are consistent with EIS measurements that show the lowest impedance for the 2 mA/cm^2 cells compared with all of the other samples, indicating that both NMR and EIS detect the resistance properties of the SEI generated during formation. Considering that each Li metal anode shows vastly different performance despite cycling in the same LP30 electrolyte, the process of electrochemical formation must lead to modifications in the SEI that dictate the energy barriers to Li transport.

Please cite this article in press as: Svirinovsky-Arbeli et al., Using NMR spectroscopy to link structure to function at the Li solid electrolyte interphase, Joule (2024), https://doi.org/10.1016/j.joule.2024.04.016

Based on cross-polarization magic-angle spinning (CPMAS) solid-state NMR experiments and XPS measurements, the authors find that electrochemical formation at 2 mA/cm^2 produces lower amounts of Li_2O and a higher amount of LiF in the SEI. They argue that by eliminating ionically insulating Li_2O, the energy barrier to Li diffusion through the interface decreases. However, we note that the activation energy for Li^+ transport in LiF is predicted to be higher than that of Li_2O,[52] and LiF notoriously suffers from low ionic conductivity.[77,78] One potential explanation for the correlation between LiF quantity and high CE could be crystallite size, grain boundaries, and/or the formation of amorphous phases, which are discussed in more detail in the next section. In addition, due to potential beam damage in XPS and the poor resolution in ^{7}Li NMR, the contribution from other phases to performance degradation may not be detected. Recent work using MS titration indicates that minor SEI components, like Li_2C_2, show a negative correlation with Li metal CE, and species like these may increase in concentration during non-ideal formation protocols.[79] The same group also used titration to show that increased Li_2O content in the SEI shows the strongest correlation with CE, even over LiF.[80] CryoEM indicates that the crystallinity of both Li_2O and LiF in the SEI varies with cycling protocol, potentially explaining some of the discrepancies observed between different labs. Next, we will describe how we can potentially leverage NMR lineshape analyses to understand these changes in crystallinity and particle size and relate this information back to transport properties in the SEI. In the end, complementing NMR techniques with more sensitive methods like MS and imaging methods may provide a route to elucidate how small quantities of electrolyte decomposition products and distinct phases impact overall performance.

UNDERSTANDING AND CONTROLLING MECHANISMS OF LI-ION TRANSPORT THROUGH THE SEI

The SEI is undoubtedly one of the most complicated and least understood aspects of the battery.[81] Compared with the solid electrodes and liquid electrolyte, it is significantly more heterogeneous (compositionally, it may exhibit both dense and porous regions), disordered (contains both amorphous and crystalline components), delicate (air sensitive, thin, and easily disrupted during sample preparation), and dynamic (continues to evolve over the course of cycling). As a result, our understanding on how specific SEI compounds and their arrangement influence Li^+ diffusion to the underlying electrode is extremely limited.

In the previous section, we saw how NMR can be used to probe both composition and Li exchange dynamics at Li anode interfaces. To confidently assign the chemical composition of the SEI, there are a multitude of complementary techniques (e.g., XPS, FTIR, and MS) that can detect both organic and inorganic electrolyte decomposition products on the electrode surface (Figure 4A). From multiple independent analyses over the past few decades, several compounds are well-accepted to form and deposit on the electrode surface in conventional carbonate electrolytes, including LEDC, LiF, Li_2O, and Li_2CO_3.[83–86] From here, one may start to deduce how individual phases contribute to Li transport and overall SEI functionality.[52,87–89] For example, Sun and coworkers used DFT to show that the energy barriers for Li migration in different SEI components exhibit the following trend where LiF > Li_2CO_3 > Li_2O (70 > 22–47 > 15 kJ/mol).[52] Of the three compounds, the properties of LiF are perhaps the most puzzling, given that a dense, LiF-rich SEI is routinely correlated with high CE in LMBs.[78] A few years later, Greeley and coworkers also found that the calculated barriers for Li^+ diffusion in bulk LiF are high (>70 kJ/mol) unless

Please cite this article in press as: Svirinovsky-Arbeli et al., Using NMR spectroscopy to link structure to function at the Li solid electrolyte interphase, Joule (2024), https://doi.org/10.1016/j.joule.2024.04.016

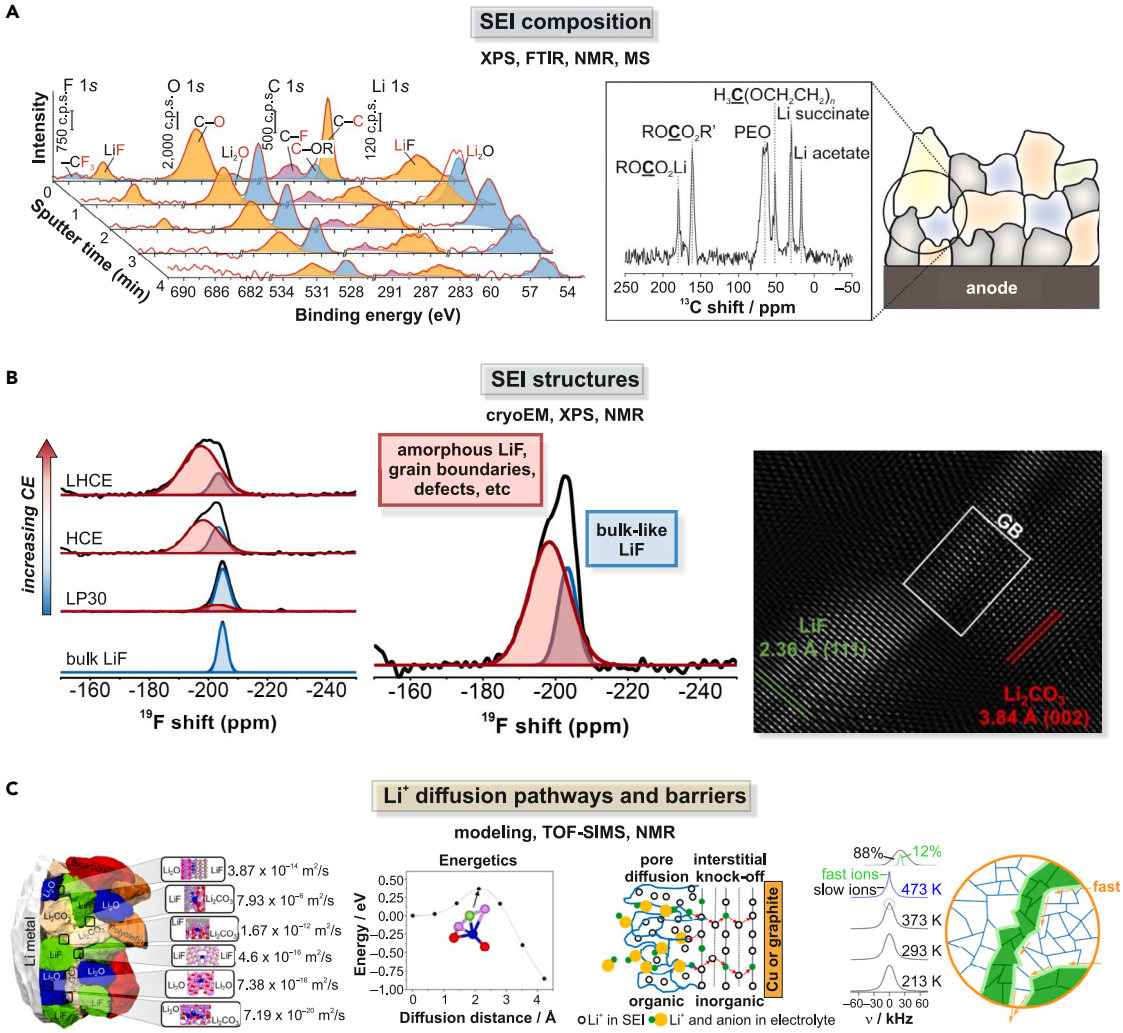

Figure 4. Multimodal approach to understanding SEI functionality

(A) A suite of chemical characterization techniques, including XPS, FTIR, NMR, and MS, are used to identify the composition of the SEI. Adapted with permission from Lin et al.,[82] Copyright 2019 Spring Nature.

(B) Local structure probes like cryo-TEM, depth profiling in XPS, and NMR are used to characterize SEI structure and can help visual grain size and local coordination environment. (Adapted with permission from Das Goswami et al.,[50] Copyright 2023 American Chemical Society.) ^{19}F NMR, in particular, can resolve and quantify F sites in LiF in different coordination environments as a function of Li CE (left and middle panels).

(C) Li diffusion pathways and associated energy barriers for Li diffusion through specific grain boundaries and SEI regions are examined with computer simulations, TOF-SIMS, and NMR. Adapted with permission from Das Goswami et al.,[50] Copyright 2023 American Chemical Society. Adapted with permission from Shi et al.,[51] Copyright 2012 American Chemical Society. Adapted with permission from Gombotz et al.,[49] Copyright 2021 Elsevier.

diffusion proceeds through an interstitial knock-off mechanism (26 kJ/mol).[90] In 2023, Wen, Xu, and coworkers decided to examine Li^+ diffusion in amorphous Li_2CO_3 and LiF rather than their crystalline analogs,[91] which may exist in thin SEI layers. Machine learning potential-assisted MD simulations indicate that Li^+ conduction in LiF is still worse than in Li_2CO_3, even in bulk amorphous phases. However, the data suggest that if LiF grain size is reduced and embedded in a Li_2CO_3-rich SEI, one may be able to retain the benefits of LiF (e.g., low electronic conductivity) while also enabling Li transport.

Although these results do not entirely explain how large quantities of LiF enable high-performance Li batteries, they point to the possibility that it is not only the

Please cite this article in press as: Svirinovsky-Arbeli et al., Using NMR spectroscopy to link structure to function at the Li solid electrolyte interphase, Joule (2024), https://doi.org/10.1016/j.joule.2024.04.016

composition of individual compounds in the SEI that dictate Li^+ diffusion, but their structures, morphologies, grain size, and grain boundaries.[21,92–94] Over the past few years, cryo-TEM has emerged as a promising technique to characterize the thickness, conformality, particle size, and distribution of crystalline and amorphous components in both the SEI and cathode electrolyte interphase (CEI). When Li metal electrodes are cycled in conventional carbonate electrolytes, the SEI often exhibits a mosaic structure with ~5–10 nm crystalline Li_2CO_3 and Li_2O particles embedded in an amorphous layer on the Li surface.[74,95,96] Interestingly, the diffraction pattern corresponding to LiF is not always observed in the SEI, but its presence has been well-established with electron energy loss spectroscopy (EELS), XPS, and solid-state NMR.[82,96–98] Once again, these data indicate that the particle size and crystallinity may be responsible for changes in electrochemical properties.

If we revisit the previous example on electrochemical formation, we will remember that formation cycles at 2 mA/cm^2 afforded high Li metal CE (~96%) in LP30 when the current density is dropped back down to 0.5 mA/cm^2. This result was independently verified in a similar electrolyte (1.2 M $LiPF_6$ in EC/EMC 3:7 + 5 wt % VC) by Xu et al., who used galvanostatic cycling and EIS to show that out of 0.1, 2, 5, and 9 mA/cm^2, conditioning at 2 mA/cm^2 led to the best subsequent Li/Cu cell performance.[99] Analysis of these Li electrodeposits with cryo-TEM revealed that the composition, size, and arrangement of the crystalline grains in the SEI change as a function of formation current density (this observation also indicates that special care must be taken to report the current density and deposition time). No crystalline components are observed until the current density reaches 2 mA/cm^2, where Li_2O and Li_2CO_3 are seen in the SEI. The authors note that no LiF is observed in the SEI layer until the highest current density tested (9 mA/cm^2) is reached, even when FEC is included as an additive, which is a well-known LiF-former. These results are similar to those reported by Cao et al., who found that despite cycling in a high-performance LHCE formulation and generating an inorganic, LiF-rich SEI seen in XPS, no crystalline inorganic components were observed in the SEI on Li metal using cryo-TEM.[98] Together, these results suggest that the nucleation and growth of certain phases in the SEI are highly dependent on applied current density and may play key roles in controlling the reversibility of Li electrodeposition.

A comparison of the solid-state ^{19}F NMR spectra of Li SEIs after cycling in different electrolytes in our laboratory indicates that there may, indeed, be structural changes to LiF that correlate with performance (Figure 4B). When Li metal anodes are cycled in conventional carbonate electrolytes (LP30), LiF in the SEI exhibits a sharp ^{19}F resonance at −204 ppm that is consistent with bulk LiF (Figure 4B), indicating that it is well ordered. Conversely, when Li metal is cycled in a high-CE electrolyte such as a high concentration electrolyte (HCE) or LHCE, the resulting ^{19}F NMR resonance corresponding to LiF shows a prominent, high-frequency shoulder. Similar shifts have been observed in ^{19}F NMR data for KF in K-ion batteries (KIBs) when cycled in electrolytes that show higher capacity retention.[100] In KIBs, the different KF species were attributed to defects in the metal fluoride phase that enabled K^+ transport through what is typically a poor ion conductor. When Li metal anodes are cycled in high-CE liquid electrolytes, the emergence of an additional shoulder that exhibits a broader linewidth than bulk LiF suggests that we may be forming an amorphous LiF phase. Other possibilities include the presence of grain boundaries and defects that may also lead to distinct F sites for LiF. The presence of amorphous LiF is consistent with recent cryo-TEM work where no crystalline phases were found upon cycling in an LHCE, despite the fact that it is known to be comprised of primarily inorganic

Please cite this article in press as: Svirinovsky-Arbeli et al., Using NMR spectroscopy to link structure to function at the Li solid electrolyte interphase, Joule (2024), https://doi.org/10.1016/j.joule.2024.04.016

compounds.[98] The new F environments generated in high-CE electrolytes may play a role in Li diffusion and improved Li plating behavior even though LiF is ionically insulating. More work is currently underway to assign these F environments and elucidate their role in Li metal battery performance.

One possible way that we can learn about how SEI constituents control Li^+ diffusion is by examining systems that actually do produce discrete crystalline domains and using those structures to create atomistic models. Two independent reports that have observed LiF, Li_2CO_3, and Li_2O in the SEI with cryo-TEM after plating Li in LP30 have used these structures to study lattice diffusion vs. grain boundary diffusion of Li^+ with DFT. In a recent study, Yurkiv and coworkers identified six different grain boundaries with cryo-TEM, with LiF(111)/Li_2CO_3(200), LiF(111)/Li_2CO_3(002), and Li_2O(111)/Li_2CO_3(111) representing the most stable interfaces (Figure 4C).[50] Of these structures, LiF(111)/Li_2CO_3(200) was predicted to have the highest Li diffusion coefficient (7.93×10^{-6} m^2/s), and both stable LiF/Li_2CO_3 grain boundaries showed low barriers to Li hopping (<40 kJ/mol, Figure 4C). All of the values for grain boundary diffusion were faster than lattice diffusion. The properties and resulting advantages of LiF/Li_2CO_3 interfaces in the SEI are consistent with earlier work, which showed that increasing the number of contacts between LiF and Li_2CO_3 creates space-charge accumulation in the SEI.[101] When the space-charge layer builds up at the LiF/Li_2CO_3 interface, Li^+ concentration increases and electronic conductivity decreases. Therefore, a compact SEI that includes many small grains to increase the contact area between LiF and Li_2CO_3 may help passivate the electrode surface, mitigate Li filament growth, and prevent continuous electrolyte consumption. However, the electronic conductivity at defects/grain boundaries is expected to be closely tied to Li filament growth,[102–104] so more work must be done to understand the relationship between interfacial structure and composition. In the work by Yurkiv and coworkers, electronic structure calculations predicted that the Li_2O(111)/Li_2CO_3(111) grain boundaries formed in conventional carbonate electrolytes may leave the system susceptible to Li metal nucleation.[50] Likewise, Qi and coworkers found that more under-coordinated atoms in grain boundaries led to smaller bandgaps,[105] suggesting that if the particle size of SEI compounds is too small, this may also lead to Li filament-driven short circuiting and low CE.

To gain deeper insight into interfacial Li diffusion mechanisms and validate computational models, high-resolution experimental methods are required to measure Li transport within the SEI. In 2012, Lu and Harris used a combination of multiscale modeling, TEM, and TOF-SIMS to study the mechanism of Li^+ transport through the SEI produced upon cycling in a $LiClO_4$-based carbonate electrolyte (Figure 4C).[51] Upon leaving the electrolyte and entering the porous, organic SEI, Li^+ diffuses quickly via pore diffusion until it reaches the dense, inorganic layer. In this electrolyte, the inner SEI is mostly comprised of Li_2CO_3 in which the authors predict that the most favorable route for Li-ion conduction is a knock-off mechanism (instead of ion hopping) with an energy barrier of 30 kJ/mol. Although this model describes the $^6Li/^7Li$ ratio observed with TOF-SIMS as a function of location in the SEI, it does not take into account the fact that this SEI also contains Li_2O. Further development of this method will likely help improve our understanding on how both organic and inorganic phases facilitate Li^+ diffusion in different electrolytes.

In addition to direct experimental probes, one can also construct prototypes to examine the functionality of SEI compounds under different conditions. In an effort

Please cite this article in press as: Svirinovsky-Arbeli et al., Using NMR spectroscopy to link structure to function at the Li solid electrolyte interphase, Joule (2024), https://doi.org/10.1016/j.joule.2024.04.016

to understand how an ionic insulator like LiF could be so ubiquitous in high-performing Li batteries, Wilkening and coworkers created a series of model systems to study Li^+ transport in LiF and its composites with solid-state NMR (Figure 4C).[48,49] In this system, the authors found that when bulk LiF is reduced to the nanometer-length scale via ball milling, the ionic conductivity increases by two orders of magnitude. Upon forming a composite of LiF and Al_2O_3 or TiO_2, conductivity increased even further. Both systems showed mobile ion fractions in ^{7}Li and ^{19}F NMR, but Li^+ was found to be the dominant charge carrier. Mixing with Al_2O_3 to form a $(LiF)_{0.86}(Al_2O_3)_{0.14}$ composite anchored F^- anions to AlO_5 units, which increased Li^+ conductivity by five orders of magnitude (at 393 K) compared with bulk LiF at the LiF/Al_2O_3 interface and dropped the activation energy for Li diffusion from 95 kJ/mol to 76 kJ/mol.[48] Similarly, ball-milling LiF with 40 wt % TiO_2 increased the ionic conductivity from 10^{-11} S/cm to 10^{-7} S/cm (at 393 K) and dropped the energy barrier to Li diffusion to 19 kJ/mol at room temperature.[49] The authors attribute these results to the large number of defect-rich space-charge regions in the composite samples that facilitate fast Li^+ transport at the interfaces and suggest that this may be a route to approach interfacial engineering.

OUTLOOK

The quest to discover an electrolyte that can enable rechargeable LMBs must come with an ability to understand its functionality if we wish to continue to accelerate the transition to renewables. In this review, we outline the ways in which NMR spectroscopy, in conjunction with other characterization techniques, can contribute to correlating material properties with electrochemical behavior. As we build on this work, there are still many aspects about interfacial chemistry that are key to Li electrodeposition and remain poorly understood. We have shown the unique power of NMR to reveal structural changes in compounds, like LiF, that are known ion insulators, in high-performance electrolytes that may be the key to unlocking Li^0 cyclability. Still, very little is known about the physical process or the energetics of transferring solvated Li^+ to the SEI and vice versa, which may play an important role in the rate of Li stripping/plating. Molecular characterization techniques like NMR, FTIR, Raman, and MS are all well-suited to characterize the solvation structure of active ions. Surface-sensitive dynamic nuclear polarization (DNP) NMR is one of the few methods that can probe the structural features of the outermost layer of the SEI to describe the chemical components involved with ion transfer, and exchange techniques may be helpful to clarify the barriers associated with desolvation when used in combination with EIS. Combining NMR with other tools (like MS titration, cryo-TEM, and computer simulations) to systematically evaluate compositional, structural, and dynamic changes in the SEI will allow us to uncover the precise chemical building blocks that enable reversible Li metal electrodeposition and expand this knowledge to new classes of energy storage systems.

ACKNOWLEDGMENTS

This work was supported by the National Science Foundation (NSF) CAREER Award (CBET-2045262) and the Research Corporation for Science Advancement through a Cottrell Scholar Award (28206). A.S.-A. is supported by the Columbia Climate School Postdoctoral Research Program at Columbia University. M.J. is supported by the Carlsberg Foundation, grant CF22-0367.

AUTHOR CONTRIBUTIONS

Conceptualization, A.S.-A. and L.E.M.; writing – original draft, A.S.-A. and L.E.M.; writing – review & editing, A.S.-A., M.J., R.M., Y.K., and L.E.M.; funding acquisition, A.S.-A., M.J., and L.E.M.; supervision, L.E.M.

DECLARATION OF INTERESTS

The authors declare no competing interests.

REFERENCES

1. Viswanathan, V., Epstein, A.H., Chiang, Y.-M., Takeuchi, E., Bradley, M., Langford, J., and Winter, M. (2022). The challenges and opportunities of battery-powered flight. Nature *601*, 519–525.
2. Chen, S., Dai, F., and Cai, M. (2020). Opportunities and Challenges of High-Energy Lithium Metal Batteries for Electric Vehicle Applications. ACS Energy Lett. *5*, 3140–3151.
3. Sripad, S., and Viswanathan, V. (2017). Performance Metrics Required of Next-Generation Batteries to Make a Practical Electric Semi Truck. ACS Energy Lett. *2*, 1669–1673.
4. Liu, J., Bao, Z., Cui, Y., Dufek, E.J., Goodenough, J.B., Khalifah, P., Li, Q., Liaw, B.Y., Liu, P., Manthiram, A., et al. (2019). Pathways for practical high-energy long-cycling lithium metal batteries. Nat. Energy *4*, 180–186.
5. Winter, M., Barnett, B., and Xu, K. (2018). Before Li Ion Batteries. Chem. Rev. *118*, 11433–11456.
6. Goodenough, J.B., and Kim, Y. (2010). Challenges for Rechargeable Li Batteries. Chem. Mater. *22*, 587–603.
7. Shan, X., Zhong, Y., Zhang, L., Zhang, Y., Xia, X., Wang, X., and Tu, J. (2021). A Brief Review on Solid Electrolyte Interphase Composition Characterization Technology for Lithium Metal Batteries: Challenges and Perspectives. J. Phys. Chem. C *125*, 19060–19080.
8. Wu, H., Jia, H., Wang, C., Zhang, J.-G., and Xu, W. (2021). Recent Progress in Understanding Solid Electrolyte Interphase on Lithium Metal Anodes. Adv. Energy Mater. *11*, 2003092.
9. Park, H., Tamwattana, O., Kim, J., Buakeaw, S., Hongtong, R., Kim, B., Khomein, P., Liu, G., Meethong, N., and Kang, K. (2021). Probing Lithium Metals in Batteries by Advanced Characterization and Analysis Tools. Adv. Energy Mater. *11*, 2003039.
10. Jin, Y., Kneusels, N.H., Magusin, P.C.M.M., Kim, G., Castillo-Martínez, E., Marbella, L.E., Kerber, R.N., Howe, D.J., Paul, S., Liu, T., and Grey, C.P. (2017). Identifying the Structural Basis for the Increased Stability of the Solid Electrolyte Interphase Formed on Silicon with the Additive Fluoroethylene Carbonate. J. Am. Chem. Soc. *139*, 14992–15004.
11. Nie, M., Abraham, D.P., Chen, Y., Bose, A., and Lucht, B.L. (2013). Silicon Solid Electrolyte Interphase (SEI) of Lithium Ion Battery Characterized by Microscopy and Spectroscopy. J. Phys. Chem. C *117*, 13403–13412.
12. Michan, A.L., Parimalam, B.S., Leskes, M., Kerber, R.N., Yoon, T., Grey, C.P., and Lucht, B.L. (2016). Fluoroethylene Carbonate and Vinylene Carbonate Reduction: Understanding Lithium-Ion Battery Electrolyte Additives and Solid Electrolyte Interphase Formation. Chem. Mater. *28*, 8149–8159.
13. Xu, K., Zhuang, G.V., Allen, J.L., Lee, U., Zhang, S.S., Ross, P.N., Jr., and Jow, T.R. (2006). Syntheses and Characterization of Lithium Alkyl Mono- and Dicarbonates as Components of Surface Films in Li-Ion Batteries. J. Phys. Chem. B *110*, 7708–7719.
14. Aurbach, D., Markovsky, B., Weissman, I., Levi, E., and Ein-Eli, Y. (1999). On the correlation between surface chemistry and performance of graphite negative electrodes for Li ion batteries. Electrochim. Acta *45*, 67–86.
15. Fan, X., Chen, L., Ji, X., Deng, T., Hou, S., Chen, J., Zheng, J., Wang, F., Jiang, J., Xu, K., and Wang, C. (2018). Highly Fluorinated Interphases Enable High-Voltage Li-Metal Batteries. Chem *4*, 174–185.
16. Miao, R., Yang, J., Feng, X., Jia, H., Wang, J., and Nuli, Y. (2014). Novel dual-salts electrolyte solution for dendrite-free lithium-metal based rechargeable batteries with high cycle reversibility. J. Power Sources *271*, 291–297.
17. Qiu, F., Li, X., Deng, H., Wang, D., Mu, X., He, P., and Zhou, H. (2019). A Concentrated Ternary-Salts Electrolyte for High Reversible Li Metal Battery with Slight Excess Li. Adv. Energy Mater. *9*, 1803372.
18. Qian, J., Henderson, W.A., Xu, W., Bhattacharya, P., Engelhard, M., Borodin, O., and Zhang, J.-G. (2015). High rate and stable cycling of lithium metal anode. Nat. Commun. *6*, 6362.
19. Suo, L., Xue, W., Gobet, M., Greenbaum, S.G., Wang, C., Chen, Y., Yang, W., Li, Y., and Li, J. (2018). Fluorine-donating electrolytes enable highly reversible 5-V-class Li metal batteries. Proc. Natl. Acad. Sci. USA *115*, 1156–1161.
20. Li, W., Yao, H., Yan, K., Zheng, G., Liang, Z., Chiang, Y.-M., and Cui, Y. (2015). The synergetic effect of lithium polysulfide and lithium nitrate to prevent lithium dendrite growth. Nat. Commun. *6*, 7436.
21. Li, T., Zhang, X.-Q., Shi, P., and Zhang, Q. (2019). Fluorinated Solid-Electrolyte Interphase in High-Voltage Lithium Metal Batteries. Joule *3*, 2647–2661.
22. May, R., Fritzsching, K.J., Livitz, D., Denny, S.R., and Marbella, L.E. (2021). Rapid Interfacial Exchange of Li Ions Dictates High Coulombic Efficiency in Li Metal Anodes. ACS Energy Lett. *6*, 1162–1169.
23. Gunnarsdóttir, A.B., Vema, S., Menkin, S., Marbella, L.E., and Grey, C.P. (2020). Investigating the effect of a fluoroethylene carbonate additive on lithium deposition and the solid electrolyte interphase in lithium metal batteries using in situ NMR spectroscopy. J. Mater. Chem. A *8*, 14975–14992.
24. Columbus, D., Arunachalam, V., Glang, F., Avram, L., Haber, S., Zohar, A., Zaiss, M., and Leskes, M. (2022). Direct Detection of Lithium Exchange across the Solid Electrolyte Interphase by ^{7}Li Chemical Exchange Saturation Transfer. J. Am. Chem. Soc. *144*, 9836–9844.
25. Gunnarsdóttir, A.B., Amanchukwu, C.V., Menkin, S., and Grey, C.P. (2020). Noninvasive In Situ NMR Study of "Dead Lithium" Formation and Lithium Corrosion in Full-Cell Lithium Metal Batteries. J. Am. Chem. Soc. *142*, 20814–20827.
26. Ganapathy, S., van Eck, E.R.H., Kentgens, A.P.M., Mulder, F.M., and Wagemaker, M. (2011). Equilibrium Lithium-Ion Transport Between Nanocrystalline Lithium-Inserted Anatase TiO_2 and the Electrolyte. Chemistry *17*, 14811–14816.
27. Zhang, S., Li, Y., Bannenberg, L.J., Liu, M., Ganapathy, S., and Wagemaker, M. (2024). The lasting impact of formation cycling on the Li-ion kinetics between SEI and the Li-metal anode and its correlation with efficiency. Sci. Adv. *10*, eadj8889.
28. Ilott, A.J., and Jerschow, A. (2018). Probing Solid-Electrolyte Interphase (SEI) Growth and Ion Permeability at Undriven Electrolyte–Metal Interfaces Using ^{7}Li NMR. J. Phys. Chem. C *122*, 12598–12604.
29. Cheng, Z., Liu, M., Ganapathy, S., Li, C., Li, Z., Zhang, X., He, P., Zhou, H., and Wagemaker, M. (2020). Revealing the Impact of Space-Charge Layers on the Li-Ion Transport in All-Solid-State Batteries. Joule *4*, 1311–1323.
30. Yu, C., Ganapathy, S., Eck, E.R.H.V., Wang, H., Basak, S., Li, Z., and Wagemaker, M. (2017). Accessing the bottleneck in all-solid state batteries, lithium-ion transport over the solid-electrolyte-electrode interface. Nat. Commun. *8*, 1086.
31. Ganapathy, S., Yu, C., van Eck, E.R.H., and Wagemaker, M. (2019). Peeking across Grain Boundaries in a Solid-State Ionic Conductor. ACS Energy Lett. *4*, 1092–1097.
32. Zheng, J., Tang, M., and Hu, Y.-Y. (2016). Lithium Ion Pathway within $Li_7La_3Zr_2O_{12}$-Polyethylene Oxide Composite Electrolytes. Angew. Chem. Int. Ed. Engl. *55*, 12538–12542.
33. Zheng, J., Dang, H., Feng, X., Chien, P.-H., and Hu, Y.-Y. (2017). Li-ion transport in a representative ceramic–polymer–plasticizer composite electrolyte: $Li_7La_3Zr_2O_{12}$–polyethylene oxide–tetraethylene glycol dimethyl ether. J. Mater. Chem. A *5*, 18457–18463.
34. Zheng, J., and Hu, Y.-Y. (2018). New Insights into the Compositional Dependence of Li-Ion Transport in Polymer–Ceramic Composite Electrolytes. ACS Appl. Mater. Interfaces *10*, 4113–4120.
35. Bogle, X., Vazquez, R., Greenbaum, S., Cresce, A.v.W., and Xu, K. (2013).

Understanding Li^+–Solvent Interaction in Nonaqueous Carbonate Electrolytes with ^{17}O NMR. J. Phys. Chem. Lett. *4*, 1664–1668.

36. May, R., Hestenes, J.C., Munich, N.A., and Marbella, L.E. (2023). Fluorinated ether decomposition in localized high concentration electrolytes. J. Power Sources *553*, 232299.

37. May, R., Zhang, Y., Denny, S.R., Viswanathan, V., and Marbella, L.E. (2020). Leveraging Cation Identity to Engineer Solid Electrolyte Interphases for Rechargeable Lithium Metal Anodes. Cell Reports Physical Science *1*, 100239.

38. Chandrashekar, S., Trease, N.M., Chang, H.J., Du, L.-S., Grey, C.P., and Jerschow, A. (2012). ^7Li MRI of Li batteries reveals location of microstructural lithium. Nat. Mater. *11*, 311–315.

39. Ilott, A.J., Mohammadi, M., Chang, H.J., Grey, C.P., and Jerschow, A. (2016). Real-time 3D imaging of microstructure growth in battery cells using indirect MRI. Proc. Natl. Acad. Sci. USA *113*, 10779–10784.

40. Girard, G.M.A., Hilder, M., Dupre, N., Guyomard, D., Nucciarone, D., Whitbread, K., Zavorine, S., Moser, M., Forsyth, M., MacFarlane, D.R., and Howlett, P.C. (2018). Spectroscopic Characterization of the SEI Layer Formed on Lithium Metal Electrodes in Phosphonium Bis(fluorosulfonyl)imide Ionic Liquid Electrolytes. ACS Appl. Mater. Interfaces *10*, 6719–6729.

41. Huff, L.A., Tavassol, H., Esbenshade, J.L., Xing, W., Chiang, Y.-M., and Gewirth, A.A. (2016). Identification of Li-Ion Battery SEI Compounds through ^7Li and ^{13}C Solid-State MAS NMR Spectroscopy and MALDI-TOF Mass Spectrometry. ACS Appl. Mater. Interfaces *8*, 371–380.

42. Krachkovskiy, S.A., Foster, J.M., Bazak, J.D., Balcom, B.J., and Goward, G.R. (2018). Operando Mapping of Li Concentration Profiles and Phase Transformations in Graphite Electrodes by Magnetic Resonance Imaging and Nuclear Magnetic Resonance Spectroscopy. J. Phys. Chem. C *122*, 21784–21791.

43. Boyle, D.T., Kim, S.C., Oyakhire, S.T., Vilá, R.A., Huang, Z., Sayavong, P., Qin, J., Bao, Z., and Cui, Y. (2022). Correlating Kinetics to Cyclability Reveals Thermodynamic Origin of Lithium Anode Morphology in Liquid Electrolytes. J. Am. Chem. Soc. *144*, 20717–20725.

44. Boyle, D.T., Kong, X., Pei, A., Rudnicki, P.E., Shi, F., Huang, W., Bao, Z., Qin, J., and Cui, Y. (2020). Transient Voltammetry with Ultramicroelectrodes Reveals the Electron Transfer Kinetics of Lithium Metal Anodes. ACS Energy Lett. *5*, 701–709.

45. Shi, F., Pei, A., Boyle, D.T., Xie, J., Yu, X., Zhang, X., and Cui, Y. (2018). Lithium metal stripping beneath the solid electrolyte interphase. Proc. Natl. Acad. Sci. USA *115*, 8529–8534.

46. Hobold, G.M., Kim, K.-H., and Gallant, B.M. (2023). Beneficial vs. inhibiting passivation by the native lithium solid electrolyte interphase revealed by electrochemical Li^+ exchange. Energy Environ. Sci. *16*, 2247–2261.

47. Ko, S., Obukata, T., Shimada, T., Takenaka, N., Nakayama, M., Yamada, A., and Yamada, Y. (2022). Electrode potential influences the reversibility of lithium-metal anodes. Nat. Energy *7*, 1217–1224.

48. Breuer, S., Pregartner, V., Lunghammer, S., and Wilkening, H.M.R. (2019). Dispersed Solid Conductors: Fast Interfacial Li-Ion Dynamics in Nanostructured LiF and LiF:γ-Al_2O_3 Composites. J. Phys. Chem. C *123*, 5222–5230.

49. Gombotz, M., Pree, K.P., Pregartner, V., Hanzu, I., Gadermaier, B., Hogrefe, K., and Wilkening, H.M.R. (2021). Insulator:conductor interfacial regions — Li ion dynamics in the nanocrystalline dispersed ionic conductor LiF:TiO_2. Solid State Ionics *369*, 115726.

50. Das Goswami, B.R., Jabbari, V., Shahbazian-Yassar, R., Mashayek, F., and Yurkiv, V. (2023). Unraveling Ion Diffusion Pathways and Energetics in Polycrystalline SEI of Lithium-Based Batteries: Combined Cryo-HRTEM and DFT Study. J. Phys. Chem. C *127*, 21971–21979.

51. Shi, S., Lu, P., Liu, Z., Qi, Y., Hector, L.G., Jr., Li, H., and Harris, S.J. (2012). Direct Calculation of Li-Ion Transport in the Solid Electrolyte Interphase. J. Am. Chem. Soc. *134*, 15476–15487.

52. Chen, Y.C., Ouyang, C.Y., Song, L.J., and Sun, Z.L. (2011). Electrical and Lithium Ion Dynamics in Three Main Components of Solid Electrolyte Interphase from Density Functional Theory Study. J. Phys. Chem. C *115*, 7044–7049.

53. Meng, Y.S., Srinivasan, V., and Xu, K. (2022). Designing better electrolytes. Science *378*, eabq3750.

54. Zhao, Y., Zhou, T., Jeurgens, L.P.H., Kong, X., Choi, J.W., and Coskun, A. (2023). Electrolyte engineering for highly inorganic solid electrolyte interphase in high-performance lithium metal batteries. Chem *9*, 682–697.

55. Hobold, G.M., Lopez, J., Guo, R., Minafra, N., Banerjee, A., Shirley Meng, Y., Shao-Horn, Y., and Gallant, B.M. (2021). Moving beyond 99.9% Coulombic efficiency for lithium anodes in liquid electrolytes. Nat. Energy *6*, 951–960.

56. Wang, H., Yu, Z., Kong, X., Kim, S.C., Boyle, D.T., Qin, J., Bao, Z., and Cui, Y. (2022). Liquid electrolyte: The nexus of practical lithium metal batteries. Joule *6*, 588–616.

57. Suo, L., Hu, Y.-S., Li, H., Armand, M., and Chen, L. (2013). A new class of Solvent-in-Salt electrolyte for high-energy rechargeable metallic lithium batteries. Nat. Commun. *4*, 1481.

58. Wang, J., Yamada, Y., Sodeyama, K., Chiang, C.H., Tateyama, Y., and Yamada, A. (2016). Superconcentrated electrolytes for a high-voltage lithium-ion battery. Nat. Commun. *7*, 12032.

59. Zeng, Z., Murugesan, V., Han, K.S., Jiang, X., Cao, Y., Xiao, L., Ai, X., Yang, H., Zhang, J.-G., Sushko, M.L., and Liu, J. (2018). Non-flammable electrolytes with high salt-to-solvent ratios for Li-ion and Li-metal batteries. Nat. Energy *3*, 674–681.

60. Ren, X., Zou, L., Cao, X., Engelhard, M.H., Liu, W., Burton, S.D., Lee, H., Niu, C., Matthews, B.E., Zhu, Z., et al. (2019). Enabling High-Voltage Lithium-Metal Batteries under Practical Conditions. Joule *3*, 1662–1676.

61. Chen, S., Zheng, J., Mei, D., Han, K.S., Engelhard, M.H., Zhao, W., Xu, W., Liu, J., and Zhang, J.-G. (2018). High-Voltage Lithium-Metal Batteries Enabled by Localized High-Concentration Electrolytes. Adv. Mater. *30*, e1706102.

62. Chen, S., Zheng, J., Yu, L., Ren, X., Engelhard, M.H., Niu, C., Lee, H., Xu, W., Xiao, J., Liu, J., and Zhang, J.-G. (2018). High-Efficiency Lithium Metal Batteries with Fire-Retardant Electrolytes. Joule *2*, 1548–1558.

63. Yang, Y., Davies, D.M., Yin, Y., Borodin, O., Lee, J.Z., Fang, C., Olguin, M., Zhang, Y., Sablina, E.S., Wang, X., et al. (2019). High-Efficiency Lithium-Metal Anode Enabled by Liquefied Gas Electrolytes. Joule *3*, 1986–2000.

64. Liu, Y., Xu, X., Sadd, M., Kapitanova, O.O., Krivchenko, V.A., Ban, J., Wang, J., Jiao, X., Song, Z., Song, J., et al. (2021). Insight into the Critical Role of Exchange Current Density on Electrodeposition Behavior of Lithium Metal. Adv. Sci. (Weinh) *8*, 2003301.

65. Zhang, X.-Q., Chen, X., Hou, L.-P., Li, B.-Q., Cheng, X.-B., Huang, J.-Q., and Zhang, Q. (2019). Regulating Anions in the Solvation Sheath of Lithium Ions for Stable Lithium Metal Batteries. ACS Energy Lett. *4*, 411–416.

66. Tao, R., Bi, X., Li, S., Yao, Y., Wu, F., Wang, Q., Zhang, C., and Lu, J. (2017). Kinetics Tuning the Electrochemistry of Lithium Dendrites Formation in Lithium Batteries through Electrolytes. ACS Appl. Mater. Interfaces *9*, 7003–7008.

67. Fan, X., Chen, L., Borodin, O., Ji, X., Chen, J., Hou, S., Deng, T., Zheng, J., Yang, C., Liou, S.-C., et al. (2018). Non-flammable electrolyte enables Li-metal batteries with aggressive cathode chemistries. Nat. Nanotechnol. *13*, 715–722.

68. Cheng, X.-B., Zhang, R., Zhao, C.-Z., and Zhang, Q. (2017). Toward Safe Lithium Metal Anode in Rechargeable Batteries: A Review. Chem. Rev. *117*, 10403–10473.

69. Zhao, Q., Stalin, S., and Archer, L.A. (2021). Stabilizing metal battery anodes through the design of solid electrolyte interphases. Joule *5*, 1119–1142.

70. Marcus, Y. (1985). Thermodynamic functions of transfer of single ions from water to nonaqueous and mixed solvents: Part 3 - Standard potentials of selected electrodes. Pure Appl. Chem. *57*, 1129–1132.

71. Mozhzhukhina, N., and Calvo, E.J. (2017). Perspective—The Correct Assessment of Standard Potentials of Reference Electrodes in Non-Aqueous Solution. J. Electrochem. Soc. *164*, A2295–A2297.

72. Parimalam, B.S., MacIntosh, A.D., Kadam, R., and Lucht, B.L. (2017). Decomposition Reactions of Anode Solid Electrolyte

Interphase (SEI) Components with $LiPF_6$. J. Phys. Chem. C *121*, 22733–22738.

73. Li, Y., Canepa, P., and Gorai, P. (2022). Role of Electronic Passivation in Stabilizing the Lithium-$Li_xPO_yN_z$ Solid-Electrolyte Interphase. PRX Energy *1*, 023004.

74. Li, Y., Li, Y., Pei, A., Yan, K., Sun, Y., Wu, C.-L., Joubert, L.-M., Chin, R., Koh, A.L., Yu, Y., et al. (2017). Atomic structure of sensitive battery materials and interfaces revealed by cryo–electron microscopy. Science *358*, 506–510.

75. Wi, T.-U., Park, S.O., Yeom, S.J., Kim, M.-H., Kristanto, I., Wang, H., Kwak, S.K., and Lee, H.-W. (2023). Revealing the Dual-Layered Solid Electrolyte Interphase on Lithium Metal Anodes via Cryogenic Electron Microscopy. ACS Energy Lett. *8*, 2193–2200.

76. Cheng, D., Wynn, T.A., Wang, X., Wang, S., Zhang, M., Shimizu, R., Bai, S., Nguyen, H., Fang, C., Kim, M.-c., et al. (2020). Unveiling the Stable Nature of the Solid Electrolyte Interphase between Lithium Metal and LiPON via Cryogenic Electron Microscopy. Joule *4*, 2484–2500.

77. Stoebe, T.G. (1967). Influence of OH^- ions on infrared absorption and ionic conductivity in lithium fluoride crystals. J. Phys. Chem. Solids *28*, 1375–1382.

78. Tan, J., Matz, J., Dong, P., Shen, J., and Ye, M. (2021). A Growing Appreciation for the Role of LiF in the Solid Electrolyte Interphase. Adv. Energy Mater. *11*, 2100046.

79. Hobold, G.M., and Gallant, B.M. (2022). Quantifying Capacity Loss Mechanisms of Li Metal Anodes beyond Inactive Li^0. ACS Energy Lett. *7*, 3458–3466.

80. Hobold, G.M., Wang, C., Steinberg, K., Li, Y., and Gallant, B.M. (2024). High lithium oxide prevalence in the lithium solid–electrolyte interphase for high Coulombic efficiency. Nat. Energy.

81. Winter, M. (2009). The Solid Electrolyte Interphase – The Most Important and the Least Understood Solid Electrolyte in Rechargeable Li Batteries. Z. Phys. Chem. *223*, 1395–1406.

82. Lin, D., Liu, Y., Li, Y., Li, Y., Pei, A., Xie, J., Huang, W., and Cui, Y. (2019). Fast galvanic lithium corrosion involving a Kirkendall-type mechanism. Nat. Chem. *11*, 382–389.

83. Peled, E., and Menkin, S. (2017). Review—SEI: Past, Present and Future. J. Electrochem. Soc. *164*, A1703–A1719.

84. Aurbach, D. (2000). Review of selected electrode–solution interactions which determine the performance of Li and Li ion batteries. J. Power Sources *89*, 206–218.

85. Heiskanen, S.K., Kim, J., and Lucht, B.L. (2019). Generation and Evolution of the Solid Electrolyte Interphase of Lithium-Ion Batteries. Joule *3*, 2322–2333.

86. Zhang, J.-G., Xu, W., Xiao, J., Cao, X., and Liu, J. (2020). Lithium Metal Anodes with Nonaqueous Electrolytes. Chem. Rev. *120*, 13312–13348.

87. Wang, A., Kadam, S., Li, H., Shi, S., and Qi, Y. (2018). Review on modeling of the anode solid electrolyte interphase (SEI) for lithium-ion batteries. npj Comput. Mater. *4*, 15.

88. Guo, R., and Gallant, B.M. (2020). Li_2O Solid Electrolyte Interphase: Probing Transport Properties at the Chemical Potential of Lithium. Chem. Mater. *32*, 5525–5533.

89. He, M., Guo, R., Hobold, G.M., Gao, H., and Gallant, B.M. (2020). The intrinsic behavior of lithium fluoride in solid electrolyte interphases on lithium. Proc. Natl. Acad. Sci. USA *117*, 73–79.

90. Yildirim, H., Kinaci, A., Chan, M.K.Y., and Greeley, J.P. (2015). First-Principles Analysis of Defect Thermodynamics and Ion Transport in Inorganic SEI Compounds: LiF and NaF. ACS Appl. Mater. Interfaces *7*, 18985–18996.

91. Hu, T., Tian, J., Dai, F., Wang, X., Wen, R., and Xu, S. (2023). Impact of the Local Environment on Li Ion Transport in Inorganic Components of Solid Electrolyte Interphases. J. Am. Chem. Soc. *145*, 1327–1333.

92. Alzate-Vargas, L., Vikrant, K.S.N., Allu, S., and Fattebert, J.-L. (2022). Atomistic modeling of LiF microstructure ionic conductivity and its influence on nucleation and plating. Phys. Rev. Materials *6*, 095402.

93. Ramasubramanian, A., Yurkiv, V., Foroozan, T., Ragone, M., Shahbazian-Yassar, R., and Mashayek, F. (2019). Lithium Diffusion Mechanism through Solid–Electrolyte Interphase in Rechargeable Lithium Batteries. J. Phys. Chem. C *123*, 10237–10245.

94. Chen, Y., Chen, Y., Wang, R., Lv, X., and Han, Y. (2022). Generation of a highly conductive and stable solid electrolyte interphase at lithium anode under additional electric filed. Chem. Eng. J. *446*, 137435.

95. Han, B., Zhang, Z., Zou, Y., Xu, K., Xu, G., Wang, H., Meng, H., Deng, Y., Li, J., and Gu, M. (2021). Poor Stability of Li_2CO_3 in the Solid Electrolyte Interphase of a Lithium-Metal Anode Revealed by Cryo-Electron Microscopy. Adv. Mater. *33*, 2100404.

96. Wang, X., Li, Y., and Meng, Y.S. (2018). Cryogenic Electron Microscopy for Characterizing and Diagnosing Batteries. Joule *2*, 2225–2234.

97. Zhang, Z., Cui, Y., Vila, R., Li, Y., Zhang, W., Zhou, W., Chiu, W., and Cui, Y. (2021). Cryogenic Electron Microscopy for Energy Materials. Acc. Chem. Res. *54*, 3505–3517.

98. Cao, X., Ren, X., Zou, L., Engelhard, M.H., Huang, W., Wang, H., Matthews, B.E., Lee, H., Niu, C., Arey, B.W., et al. (2019). Monolithic solid–electrolyte interphases formed in fluorinated orthoformate-based electrolytes minimize Li depletion and pulverization. Nat. Energy *4*, 796–805.

99. Xu, Y., Wu, H., Jia, H., Zhang, J.-G., Xu, W., and Wang, C. (2020). Current Density Regulated Atomic to Nanoscale Process on Li Deposition and Solid Electrolyte Interphase Revealed by Cryogenic Transmission Electron Microscopy. ACS Nano *14*, 8766–8775.

100. Ells, A.W., May, R., and Marbella, L.E. (2021). Potassium Fluoride and Carbonate Lead to Cell Failure in Potassium-Ion Batteries. ACS Appl. Mater. Interfaces *13*, 53841–53849.

101. Zhang, Q., Pan, J., Lu, P., Liu, Z., Verbrugge, M.W., Sheldon, B.W., Cheng, Y.-T., Qi, Y., and Xiao, X. (2016). Synergetic Effects of Inorganic Components in Solid Electrolyte Interphase on High Cycle Efficiency of Lithium Ion Batteries. Nano Lett. *16*, 2011–2016.

102. Gorai, P., Famprikis, T., Singh, B., Stevanović, V., and Canepa, P. (2021). Devil is in the Defects: Electronic Conductivity in Solid Electrolytes. Chem. Mater. *33*, 7484–7498.

103. Han, F., Westover, A.S., Yue, J., Fan, X., Wang, F., Chi, M., Leonard, D.N., Dudney, N.J., Wang, H., and Wang, C. (2019). High electronic conductivity as the origin of lithium dendrite formation within solid electrolytes. Nat. Energy *4*, 187–196.

104. Liu, X., Garcia-Mendez, R., Lupini, A.R., Cheng, Y., Hood, Z.D., Han, F., Sharafi, A., Idrobo, J.C., Dudney, N.J., Wang, C., et al. (2021). Local electronic structure variation resulting in Li 'filament' formation within solid electrolytes. Nat. Mater. *20*, 1485–1490.

105. Feng, M., Pan, J., and Qi, Y. (2021). Impact of Electronic Properties of Grain Boundaries on the Solid Electrolyte Interphases (SEIs) in Li-ion Batteries. J. Phys. Chem. C *125*, 15821–15829.